HAL
archives-ouvertes.fr

Contribution of peatland permafrost to dissolved organic matter along a thaw gradient in North Siberia

Laure Gandois, Alison Hoyt, Christine Hatté, Laurent Jeanneau, Roman Teisserenc, Marine Liotaud, Nikita Tananaev

▶ **To cite this version:**

Laure Gandois, Alison Hoyt, Christine Hatté, Laurent Jeanneau, Roman Teisserenc, et al.. Contribution of peatland permafrost to dissolved organic matter along a thaw gradient in North Siberia. Environmental Science & Technology, American Chemical Society, 2019, 53 (24), pp.14165-14174. 10.1021/acs.est.9b03735 . insu-02358892

HAL Id: insu-02358892
https://hal-insu.archives-ouvertes.fr/insu-02358892

Submitted on 12 Nov 2019

HAL is a multi-disciplinary open access archive for the deposit and dissemination of scientific research documents, whether they are published or not. The documents may come from teaching and research institutions in France or abroad, or from public or private research centers.

L'archive ouverte pluridisciplinaire **HAL**, est destinée au dépôt et à la diffusion de documents scientifiques de niveau recherche, publiés ou non, émanant des établissements d'enseignement et de recherche français ou étrangers, des laboratoires publics ou privés.

Environmental Science & Technology

Subscriber access provided by SCD Université de Rennes1 | SCD de l'Université de Rennes 1

Characterization of Natural and Affected Environments

Contribution of peatland permafrost to dissolved organic matter along a thaw gradient in North Siberia

Laure Gandois, Alison May Hoyt, Christine Hatté, Laurent Jeanneau, Roman Teisserenc, Marine Liotaud, and Nikita Tananaev

Environ. Sci. Technol., **Just Accepted Manuscript** • DOI: 10.1021/acs.est.9b03735 • Publication Date (Web): 11 Nov 2019

Downloaded from pubs.acs.org on November 12, 2019

Just Accepted

"Just Accepted" manuscripts have been peer-reviewed and accepted for publication. They are posted online prior to technical editing, formatting for publication and author proofing. The American Chemical Society provides "Just Accepted" as a service to the research community to expedite the dissemination of scientific material as soon as possible after acceptance. "Just Accepted" manuscripts appear in full in PDF format accompanied by an HTML abstract. "Just Accepted" manuscripts have been fully peer reviewed, but should not be considered the official version of record. They are citable by the Digital Object Identifier (DOI®). "Just Accepted" is an optional service offered to authors. Therefore, the "Just Accepted" Web site may not include all articles that will be published in the journal. After a manuscript is technically edited and formatted, it will be removed from the "Just Accepted" Web site and published as an ASAP article. Note that technical editing may introduce minor changes to the manuscript text and/or graphics which could affect content, and all legal disclaimers and ethical guidelines that apply to the journal pertain. ACS cannot be held responsible for errors or consequences arising from the use of information contained in these "Just Accepted" manuscripts.

is published by the American Chemical Society. 1155 Sixteenth Street N.W., Washington, DC 20036

Published by American Chemical Society. Copyright © American Chemical Society. However, no copyright claim is made to original U.S. Government works, or works produced by employees of any Commonwealth realm Crown government in the course of their duties.

Contribution of peatland permafrost to dissolved organic matter along a thaw gradient in North Siberia

Laure Gandois[1], Alison May Hoyt[2,3], Christine Hatté[4], Laurent Jeanneau[5], Roman Teisserenc[1], Marine Liotaud[5], Nikita Tananaev[6]*

[1] EcoLab, Université de Toulouse, CNRS, INPT, UPS, Toulouse, France
[2] Max Planck Institute for Biogeochemistry, Hans-Knöll-Straße 10, Jena, Germany
[3]Lawrence Berkeley National Laboratory, Berkeley, California, USA
[4] LSCE, UMR8212 CEA/CNRS/UVSQ, Université Paris Saclay, Gif-sur-Yvette, France
[5] Université de Rennes, CNRS, Géosciences Rennes, UMR 6118, F-35000 Rennes, France
[6] Melnikov Permafrost Institute, Siberian Branch, Russian Academy of Sciences, Yakutsk, Russia

*Corresponding author. laure.gandois@ensat.fr

ABSTRACT

Permafrost peatlands are important carbon stocks currently experiencing rapid evolution after permafrost thaw. Following thaw, dissolved organic matter (DOM) is a potentially important pathway for the release of permafrost carbon. This study investigates the origin and composition of DOM across sites at different stages of thaw in a discontinuous permafrost area of North Siberia. We determine the optical properties, molecular composition, stable ($\delta^{13}C$) and radiocarbon (^{14}C) content of DOM. Early stages of thaw are characterized by high DOC concentrations, high aromaticity, contribution of vegetation-derived DOM, and a high contribution of permafrost carbon. In contrast, in later stages, the microbial contribution to DOM increases, and only modern carbon is detected. This work links DOM composition with its radiocarbon content in permafrost peatlands. It shows that DOM originating from previously

frozen permafrost peatland is highly aromatic and previously processed. It highlights the variability of post-thaw carbon dynamics in boreal and arctic ecosystems.

KEYWORDS: Permafrost peatlands, Thermokarst Bogs, Dissolved Organic Matter, Radiocarbon, Optical properties of DOM, Molecular composition of DOM, Siberia

I. Introduction

In warming boreal and arctic regions, permafrost thaw is expected to affect ecosystems storing half of the global soil organic carbon stock[1]. Permafrost thaw, a deepening of the active layer or complete disappearance of frozen layers, exposes this carbon stock to microbial decomposition. The potential release of this large sequestered organic carbon stock into the active carbon cycle as a result of warming could be a significant positive feedback to climate change[2–4]. Dissolved organic matter (DOM) is the most dynamic but least characterized carbon pool in boreal and arctic terrestrial ecosystems, and is a potentially important conduit for the release of permafrost carbon following thaw. Estimates of DOM transfer from large Arctic Rivers to the Arctic Ocean range from 25-36TgC yr^{-1}[5]. However, the overall transfer from terrestrial ecosystems to surface water is higher, as a fraction of DOM is mineralized or buried in sediments before reaching the Arctic Ocean[6]. These processes are highly dependent on DOM composition. Therefore, investigating the composition, carbon origin, and potential lability of DOM is crucial to understand the strength of potential feedbacks to climate change as a result of permafrost thaw[7]. In landscapes dominated by permafrost degradation, radiocarbon (^{14}C) measurements of the carbon released as DOM provide a powerful tool to identify shifts in carbon origin. In particular, they can help identify old permafrost-derived carbon, or carbon which has been more recently fixed from the atmosphere by vegetation, with very different implications for feedback to climate.

To date, most studies of radiocarbon content of DOM in the boreal and arctic areas have focused on rivers and streams[5,8,9]. At the outlet of large Arctic Rivers, the majority of organic carbon exported during the spring flood is young carbon. Older carbon, which may reflect permafrost thaw and/or deeper water flows is exported during low flow periods[5,10], and also found upstream in the fluvial network[6]. Despite the important role of headwaters, little research has been done in upstream catchments to characterize DOM composition and origin, or to track permafrost carbon in DOM before its signal disappears as a result of dilution, photodegradation and/or microbial consumption[11].

Permafrost peatlands are disproportionally important landscapes to study permafrost degradation, as they show the highest carbon density of boreal and artic soil, and store at least one third of the permafrost soil organic carbon stocks[1,12]. Furthermore, their degradation as a result of permafrost thaw has increased in recent decades[13,14]. Following permafrost thaw, ground subsidence and changes in hydrological pathways often lead to the formation of small thermokarst bogs nested in permafrost peatland mounds (palsa), then to larger bogs, and ultimately to inundated fens[15]. The composition of DOM evolves with this ecosystem transition, reflecting the increased contribution of new vegetation[16], microbial activity[17,18], and the transition from bog to fen[19].

Although carbon-rich permafrost peatlands account for 19% of permafrost area[15,20], the links between DOM composition, lability and origin have not been established in this context. Permafrost soils have a wide variety of formation histories and geologies[21], with important implications for organic matter composition and degree of processing prior to thaw, and potential lability after thaw[20,22]. For example, in studies of ice-rich Yedoma permafrost, ancient organic matter locked in permafrost contained high levels of small molecular weight organic acids, characterized by a low aromaticity, and was highly labile. It was therefore rapidly consumed by microorganisms and released to the atmosphere after thaw[11,23]. The link between

permafrost-derived carbon in DOM and its composition remains underexplored in peatland permafrost context.

In a discontinuous permafrost area in Northern Siberia, where permafrost peatland degradation has been recently documented, we investigate the evolution of DOM using a combination of analytical techniques from the bulk (isotopic and optical) to molecular scale, in combination with radiocarbon measurements, which are indicative of the age and origin of DOM, across thermokarst bogs and lakes of different sizes and degrees of thaw. The objectives of this study are (1) to characterize DOM composition in a thawing permafrost landscape and (2) to evaluate the influence of permafrost carbon on the composition of DOM.

II. Material & Methods

1. Study site

The study area is located near Igarka (Figure 1a), on the eastern bank of the Yenisei River (67°27’11’’N, 86°32’07’’E), in a region of discontinuous permafrost. The mean annual air temperature from 1980-2010 is -7.7±1.1 °C and the mean annual precipitation is 632±86 mm, including 320±50 mm in the form of snow[24]. Sampling focused on the Graviyka catchment (Figure 1b). The Graviyka River, with watershed of 320 km^2, is one of the northernmost tributaries of the Yenisei River. It is mainly covered by forest, dominated by larch (*Larix siberica*), birch (*Betula pendula*), and Siberian pine (*Pinus siberica*), and palsa landscapes (frozen peat mounds). The palsa landscapes are dominated by moss, lichens and small birch. Degraded areas affected by permafrost thaw are characterized by depression (thermokarsts), where thermokarst bogs dominated by *Sphagnum* spp. and *Eriophorum spp* develop. The land cover is an indicator of the permafrost status and the depth of the active layer (seasonally thawed soil layer). Forested areas tend to have a deep active layer thickness associated with Pleistocene permafrost, while palsa dominated landscapes are indicative of the presence of Holocene permafrost, with a shallower active layer depth. At our study site, peatland accumulation began

during the mid-Holocene [25,26], likely between 4 to 5 kyr BP. North of Igarka, permafrost aggradation and palsa formation occurred between 3.5 and 2.5 kyr during a period of a period of relatively cooler temperatures [27]. At our site, radiocarbon data acquired close to the active layer depth are consistent with these findings, and suggest that permafrost aggradation may have begun around 2.8 ka (Figure SI.1). Permafrost degradation, characterized by the increase of the active layer and in the region surrounding Igarka has been observed for the last 30 years [24].

2. Sample collection

In the thawing palsa areas surrounding Igarka, we sampled sites at different stages of thaw in July 2015 and July 2016, including thermokarst bogs of various sizes, a fen, and thermokarst lakes. Thermokarst bogs form in depressions where palsa thaws and collapses. At the beginning of thaw process, small thermokarst bogs form, perched on palsa mounds. As the thaw process progresses, the size of thermokarst bogs increases. A continuation of the thaw process leads to the formation of fens[15,28,29]. In addition to the size of thermokarst features, the different thaw stages are characterized by differences in dominant vegetation, with a shift from plant communities which prefer dry growing conditions to those which prefer wet growing conditions[15,16,29].

These selected sites were not intended to represent a time-since-thaw chronosequence. Instead, they were selected to represent a range of thaw-affected landscapes present in the region, from those least affect by thaw (small bogs), to larger thermokarst features which do not retain permafrost (fen and lakes). Our sampling follows the classification defined by Hodgkins et al. (2016)[16], with adaptations to our site. We sampled “small bogs”, thermokarst bogs perched on palsa, with a size < 40 m^2 (corresponding to “recently thawed palsa”). We also sampled “large bogs”, which were >100 m^2 and adjacent to small amounts of remaining palsa (corresponding to “thawing Sphagnum-dominated bogs”). The surface area of the sampled bogs

was determined based on field measurements for the smallest bogs, and using Google Earth for the larger bogs. A large (area ~ 3000 m^2) thermokarst bog developed in a mineral soil context was also sampled as a reference free from permafrost peatland carbon (referred to as MB or "mineral-context bog"). All the sampled bogs are colonized by *Sphagnum*, and the large bogs included *Eriophorum*. We also sampled a fen, in which both *Sphagnum* and *Carex* are found. In all thermokarst bogs, porewater profiles were collected in the active layer and to maximum depth of 2 m using narrow piezometers (0.64 cm diameter) connected to a hand pump. Following in situ pH and conductivity measurements, samples were filtered using pre-combusted GF/F filters and stored in cleaned (acid washed and combusted) amber glass bottles for DOC, δ^{13}C-DOC, ^{14}C-DOM, molecular and optical properties of DOM.

3. Sample analyses and calculations

3.1 DOC concentrations

Non-purgeable organic carbon (NPOC, referred to hereafter as DOC) was analyzed on filtered (GF/F Whatman) samples after acidification to pH 2 (HCl) with a TOC-V CSH analyzer (Shimadzu, Japan), with a quantification limit of 1 mg L^{-1}. Certified materials (ion 915 and ion 96.4, Environment and Climate Change Canada, Canada) were included in the analytical loop and recovery was >95% of the certified value.

3.2 Optical properties of DOM

The UV absorption spectra from 240 to 700 nm of porewater were measured with a spectrophotometer (Secoman UV light XT5), in a 1 cm quartz cell. The baseline was determined with ultra-pure water. The Specific UV Absorbance at 254 nm ($SUVA_{254}$, L mg^{-1} m^{-1}) was calculated as follows: $SUVA = A_{254}/b * [DOC]$ (L mg^{-1} m^{-1}), where A_{254} is the sample absorbance at 254 nm (non-dimensional), b is the optical path length (m) and DOC is in mg L^{-1}. SUVA is a proxy for DOM aromaticity[30]. Fluorescence measurements were performed using

a spectrofluorometer (Synergy MX, Biotek). The emission spectrum was recorded for a 370 nm excitation wavelength. The fluorescence Index (FI) was determined for a 370 nm excitation wavelength, as the ratio of the 470 nm emission and 520 nm emission, as defined by McKnight et al. (2001)[31] and Jaffé et al (2008)[32]. Potential additional absorbance related to Fe content was checked on a few samples following the procedure described by Poulin et al[33]. The additional absorbance 1.4 ± 1.6% across all samples where Fe was measured, and was therefore neglected.

3.3 Stable isotopes analysis

The δ^{13}C-DOC was analyzed at the UC Davis stable isotope facility. The analyses were performed using a O.I. Analytical Model 1030 TOC Analyzer (Xylem Analytics, College Station, TX) interfaced to a PDZ Europa 20-20 isotope ratio mass spectrometer (Sercon Ltd., Cheshire, UK) utilizing a GD-100 Gas Trap Interface (Graden Instruments). Reference materials included IAEA-600, USGS-40, USGS-41, Elemental Microanalysis (EM) reference materials, and NIST 8559, 8560, and 8561. The replicates analysis showed an average of 0.25 variation, i.e 0.16 ‰.

3.4 Radiocarbon analysis and calculation of permafrost carbon contribution

The radiocarbon content of DOM and soil organic matter (SOM) was measured on selected freeze-dried samples at the LSCE laboratory (GifA and ECHo) on the MICADAS compact AMS system[34]. From 2 to 4 samples per profile were analyzed. DOM samples were analyzed through the EA-GIS coupling[35]. For SOM values, bulk samples were analyzed. For DOM, the freeze-dried powder was analyzed. The δ^{13}C value of the freeze-dried powder was compared to the direct analysis of δ^{13}C-DOM on the liquid sample after acidification, to evaluate the need for removal of inorganic carbon. Typically, 0.5 mg of sample material was prepared in a tin capsule, and acidified with 3µL of HCl 1M. All samples were duplicated, and reproducibility of duplicates was checked (Chi2 test). Blanks and standard material (C7 and OXA2 oxalic acid)

were included in the analysis sequence. All ^{14}C results were corrected for isotopic fractionation according to the conventions of Stuiver et al (1977)[36] and reported as $F^{14}C$ following the recommendation of Reimer et al. (2004)[37].

In order to assess the contribution of permafrost carbon to individual DOM samples, a two component mixing model (permafrost and atmospheric pools) was applied to the bulk $F^{14}C$ content. The permafrost pool was determined based on 3 samples from deep frozen palsa (3 to 4 meters, SI), with an average radiocarbon content of $F^{14}C = 0.608 \pm 0.022$ (4000±290 BP). For the atmospheric pool, 36 independent calculations were performed to represent different possible atmospheric end members, as the radiocarbon content in the atmosphere has changed slightly. Plant material derived from recent photosynthesis will therefore likely represent a mix of these values, including vegetation grown over a range of recent years. Our calculations used atmospheric end members which ranged from the average atmospheric signature from 1980 to 2015 ($F^{14}C$=1.12; represents a mix of vegetation inputs over the time period) to a pure 2015 signal ($F^{14}C$= 1.02; input from the most recent 2015 vegetation only) [38] to account for the possibility of a mix of recent inputs. The proportion of permafrost carbon calculated as follows:

$$\alpha_{perm} = \frac{(F14C_{mes} - F14C_{Atmo})}{(F14C_{Perm} - F14C_{Atmo})}$$

3.5 Molecular analysis and molecular indicators calculations

In order to specifically track permafrost influence on DOM composition, a subset of samples was selected based on their ^{14}C content for molecular analysis. The thermochemolysis using tetramethylammonium hydroxide coupled to gas chromatography and mass spectrometry (THM-GC-MS) was performed according to Jeanneau et al., (2014)[39]. Briefly, approximately 1 mg of freeze-dried solid residue was introduced into an 80 µL stainless steel reactor with an excess of tetramethylammonium hydroxide (6 mg). THM reaction was performed on-line using a vertical micro-furnace pyrolyzer PZ-2020D (Frontier Laboratories, Japan) operating at

196 400°C. The products of this reaction were injected into a gas chromatograph (GC) GC-2010
197 (Shimadzu, Japan) equipped with a SLB 5MS capillary column in the split mode (60 m × 0.25
198 mm ID, 0.25 μm film thickness). Compounds were detected using a QP2010+ mass
199 spectrometer (MS) (Shimadzu, Japan) operating in the full scan mode. The list of analyzed
200 compounds and m/z ratios used for their integration are given in the supplementary materials
201 (Table SI.1). Compounds were identified on the basis of their full-scan mass spectra by
202 comparison with the NIST library and with published data[40].

203 The peak area of the selected m/z (mass/charge) for each compound was integrated and
204 corrected by a mass spectra factor calculated as the reciprocal of the proportion of the fragment
205 used for the integration and the entire fragmentogram provided by the NIST library. The
206 proportion of each compound class was calculated by dividing the sum of the areas of the
207 compounds in this class by the sum of the peak areas of all analyzed compounds expressed as
208 a percentage. The analytical uncertainty for this analytical method, expressed as a relative
209 standard deviation, ranged from 10 to 20% depending on the samples and the target compounds.

210 Target compounds were classified into four categories: small organic acids (SA), α,ω-
211 diacids containing from 4 (fumaric and succinic acids) to 6 (methylglutaric acid) carbon atoms,
212 phenolic compounds (PHE) including lignin and tannin markers, carbohydrates (CAR)
213 (deoxysaccharinic acids produced by the THM of free monosaccharrides and terminal
214 monosaccharides from polysaccharides)[41] and fatty acids (FA), from 8 to 30 carbon atoms. The
215 distribution of target compounds in these categories was used to investigate DOM origin (plant
216 vs microbial origin). The distribution of LMWFA (low molecular weight fatty acids, <C18)
217 was used as an indication of microbial activity. With the exception of n-C16 and n-C18 that can
218 derive from plant-derived input, LMWFA with more than 13 carbon atoms are known as
219 phospholipid fatty acids and serve as specific microbial biomarkers[42]. The proportion of plant-
220 derived compounds (%VEG) was calculated using the deoxyC6/C5 ratio[43] and the proportion

of plant-derived fatty acids calculated as the proportion of HMW FA among FA excluding n-C16 and n-C18[39]. Ratios of cinnamyl to vanillyl units (C/V) and of aldehyde to acid moieties for vanillyl ($(Al/Ac)_V$) and syringyl ($(Al/Ac)_S$) depend on their botanical origin or, if the botanical origin can be assumed to be constant, on their biodegradation state. As the botanical origins of our samples were homogeneous, their ratios were used as biodegradation indices based on the preferential biodegradation of (i) cinnamyl moieties and (ii) aldehydes among vanillyl and syringyl units[44,45].

4. Statistical analysis

Statistical analysis was performed using R[46] and the Rstudio software (Version 1.2.1335), using ggplot[47], dplyr[48], dunn.test[49] packages. Significant differences ($\alpha<0.05$) between groups were performed using Kruskall Wallis and Dunn's post hoc multiple test.

III. Results & Discussion

1. Evolution of DOM composition along a permafrost thaw gradient

We observe clear changes in both DOC concentration and DOM composition following permafrost peatland degradation (Table 1 &2, Figure 2). These are associated with a specific DOM composition as indicated by consistent isotopic, optical and molecular analyses. Significant relationships were observed between bulk optical properties and molecular analysis. The SUVA index was positively correlated to % PHE ($r^2 = 0.48$; $p<0.05$) and phenol ratios ($(Al/Ac)_V$ given as an example, $r^2 = 0.47$; $p<0.05$) while FI was positively correlated to the percentage of low molecular weight fatty acids (LMWFA) ($r^2 = 0.5$; $p<0.05$) and negatively with the calculated percentage of vegetation origin ($r^2 = 0.42$; $p<0.05$).

During the initial stages of thaw, in small thermokarst bogs, we measure high DOC concentrations (44.1±10.1 mg L^{-1}), (Table 1, Figure 2). In these small thermokarst bogs, DOM originates from vegetation and is highly aromatic. This is revealed by significantly lower

fluorescence index values (1.35 ± 0.06) [50], higher value of the % VEG index, and higher SUVA index values (5.4 ± 0.6 L mg^{-1} m^{-1}). This corresponds to almost 40% aromatic moieties[30], consistent with a higher proportion of phenols (PHE). The high δ^{13}C-DOC values (-27.7 ± 0.3 ‰) we observe in small thermokarst bogs are also typical of terrestrial SOM, which has been through oxidation processes. This is further confirmed by lower values of $(Al/Ac)_V$, $(Al/Ac)_S$ and C/V [51,52]. The significant correlations of $(Al/Ac)_S$ with C/V($r^2 = 0.82$; $p = 0.001$) and $(Al/Ac)_V$ ($r^2 = 0.83$; $p = 0.01$) underline the consistency between these three ratios, which supports their use as biodegradation indices (Figure SI 2).

Along the thaw gradient, in larger thermokarst bogs as well as sites that have transitioned to fens and lakes, the composition and origin of DOM evolves. DOC concentrations decrease to 16.7±1.2 mg L^{-1} in large bogs to 11.0 ± 2.4 mg L^{-1} in fens. Slightly higher values are measured in thermokarst lakes (14.0 ± 4.0 mg L^{-1}) and in the bog developed in mineral soil context (12.9 ± 2.3 mg L^{-1}). Dissolved organic matter composition evolves, with an increased proportion of microbially-derived compounds in large bogs, fens, and thermokarst lakes. This is evidenced by the increase in the fluorescence index values. The aromaticity of DOM decreases from 60 to 25%, as indicated by the SUVA index. The δ^{13}C-DOC values also decrease to -30 ‰, reaching relatively depleted values, closer to recently produced vegetation, and indicative of lower rates of processing.

Shifts of DOM composition after permafrost thaw have been reported at other boreal and arctic sites. They have been related to photodegradation, microbial activity, or change of vegetation. Laurion and Mladenov (2013)[53] showed that in the case of thawing ponds in the Canadian high Arctic, UV mostly transformed aromatic and terrestrially derived DOM into more labile molecules. More precisely, an FT-ICR-MS study of the phototransformation of DOM originating from the active layer and permafrost in Alaska[54], showed that a small proportion of molecules, holding carboxylic groups, participated in photo-oxidation. However,

in the context of thermokarst bogs, photo-oxidation is likely to be highly limited since a vegetation mat covers the surface, and this process is only likely to occur in open water. In Central Siberia[17], a decrease in the DOC concentration in thermokarst lakes was linked with a decrease in the size of organic molecules. Pokrovsky et al. (2011)[17] attributed this trend to the progressive consumption of DOM by heterotrophic bacteria and release of exometabolites by phytoplankton. Hodgkins et al (2016)[16] also reported a shift in the elemental and optical properties of DOM along a permafrost thaw gradient from thermokarst bog to fen in Sweden. The primary changes observed between the early stages of palsa thaw and the fen was the decrease of tannin-like and high O/C compounds and the increase of microbially derived DOM. These differences were mainly attributed to the presence or absence of sphagnum. In our study, a similar shift from terrestrial to microbially-derived DOM is observed from thermokarst bogs to fen, although sphagnum was present at all sites. We demonstrate in this study that the origin of DOM, traced using ^{14}C-DOM, also contributes to the shift in DOM composition.

2. Peatland permafrost influence on DOM composition: Link to potential lability

We observe that the contribution of permafrost carbon to DOM decreases along the thaw gradient, and controls DOM composition. This is revealed by the evolution of the radiocarbon content of DOM (Figure 3a&b). The lowest values of $F^{14}C$ of DOM are measured in small thermokarst bogs ($F^{14}C = 0.799 \pm 0.008$ (1800 ± 85 BP)), which correspond to a contribution of 40 to 60 % permafrost carbon. In large thermokarst bogs, the $F^{14}C$ value covers a wide range of values, depending on sample depth (from $F^{14}C = 0.842 \pm 0.005$ (1385 ± 45 BP) to $F^{14}C = 1.043 \pm 0.005$, modern carbon), with a higher contribution of permafrost carbon in deep layers. In thermokarst lakes, surface samples are characterized by modern DOM (permafrost contribution does not exceed 10 %), while old DOM ($F^{14}C = 0.854 \pm 0.008$, 1275 ± 70 BP) is measured in sediment porewater at a depth of 1 m. In the thermokarst bog developed in the mineral context, modern DOM is analyzed to depths of 2 m, and slightly lower values are

measured ($F^{14}C = 0.958 \pm 0.008$, 350 ± 65 BP). No calculation is performed for the bog developed on mineral soils, since the permafrost signature for the mineral context was not measured.

We observe that the amount of permafrost peatland carbon remaining in the sampled DOM directly influences DOM composition (Figure 4). A significant negative correlation is observed between ^{14}C-DOM and FI, as well as the percentage of vegetation. A positive correlation is highlighted between ^{14}C-DOM and SUVA index and PHE ratios ($(Al/Ac)_V$ given as an example). This reveals that a higher proportion of permafrost carbon in DOM is associated with a larger proportion of plant-derived DOM, higher aromaticity and a higher degradation state of phenols. As the proportion of permafrost carbon decreases, the microbial contribution to DOM increases.

The fact that only modern DOM is detected in fens and thermokarst lakes could mean that permafrost-derived DOM has been transferred to the fluvial network, has been diluted by modern sources of DOM in the ecosystem or has been processed on site. At our study site, no surface water connection is observed between the small and large thermokarst bogs and the fluvial network, so it is unlikely that it is transferred to surface waters. Our results suggest that the lability of permafrost peatland derived DOM is limited. Biodegradability of DOM is not strictly determined by its chemical composition, but also depends on environmental factors, such as nutrients, oxygen content or temperature [7,55]. DOM composition and the anoxic conditions may have suppressed the mineralization rate of permafrost DOM, potentially explaining its high proportion in deep layers of thermokarst bogs. However, several studies have linked higher degradability of DOM to lower aromaticity [6,7,11,56], and lower degradation states of phenols[6,57], inferring limited lability of peatland permafrost DOM at our site. However, since no direct measurement were made, the fate of DOM originating from permafrost remains uncertain. In Canada, only modern carbon was measured in CO_2 emitted from both young and

mature thermokarst bogs[58], showing that mineralization of permafrost carbon in the case of thermokarst bogs was limited. In the fen and thermokarst lakes, we detect only modern, microbially dominated DOM. However, we cannot differentiate between dilution of the permafrost signal by this modern source of DOM and on-site processing of DOM. These two processes would both result in the same observation of more modern carbon (increasing radiocarbon content) with decreasing DOC concentrations (Figure SI.3). Further work to address this ambiguity and confirm the low lability we infer from our analysis in permafrost peatlands should include the additional investigation of biodegradable DOC[59], as well as measurements of the ^{14}C content of GHGs emitted from permafrost peatlands[60].

3. DOM composition and ^{14}C content: Variability across geological context and spatial scales in the Arctic

Our work links the DOM composition with its ^{14}C content in the context of permafrost peatlands. Establishing this link between the ^{14}C-DOM (and therefore the permafrost carbon contribution to DOM) and its composition is key to assessing the potential feedback of permafrost thaw to climate change. In the Arctic, fewer studies have coupled radiocarbon content of DOM to its molecular or elemental composition[5,11,61], compared to the optical properties of DOM [5,9,11,18,61,62]. Establishing a relationship between these cheap and widely measured parameters and ^{14}C content would allow more widespread assessment of the release of old permafrost carbon following thaw. In addition, our study highlights significant relationships between SUVA and the molecular composition of DOM, especially phenol content and their degradation state, increasing the information given by such an optical index. Such relationships have been established in Alaska, for the hydrophobic fraction of DOM, with older DOM being associated with lower SUVA[9].

In contrast to studies of permafrost in other geological context[62], in our study we observe higher SUVA values (higher aromaticity) in samples with a larger proportion of permafrost

DOM (Figure 5). In existing Arctic studies, none of which were conducted on permafrost peatlands, a larger permafrost influence (lower radiocarbon content) correlates with lower SUVA values, indicating a lower aromaticity and higher lability[6] (Figure 5 and Table 3). In the case of the Yenisei catchment in Siberia, shifts of DOM bulk age are related to hydrology, with young DOM being exported during spring snowmelt. This spring DOM originates from the flushing of fresh litter and shallow organic soil layers, and therefore has a more aromatic composition[10]. In the context of Yedoma, permafrost has been shown to have sequestered high content of aliphatic and small organic acids. For example in an Alaskan core, 24% of permafrost dissolved organic carbon was found in the form of highly labile acetate[63], consumed within days. This explains the low SUVA associated with the older samples, and the high lability[6]. In the case of high Canadian Arctic ponds[18], DOM from thawing ponds is a mixture of old DOM and autochthonous DOM, resulting in a low apparent SUVA of old DOM.

The apparent contradiction between the trends in these studies and our own observations (Figure 5) can likely be explained by the geological context, permafrost history and scale of our study. In addition, the peatland type[20] and the history of permafrost formation[22] could influence organic matter composition and lability in permafrost peatlands. At our study site, peatland formation during the Holocene was followed by permafrost aggradation[27]. Therefore, the formation of permafrost likely froze highly aromatic organic matter, which is typical of peatlands. This organic matter might have already undergone microbial processing over long periods, perhaps further increasing the aromaticity of DOM[64]. This would explain the observed characteristics of old bulk DOM in our study, and a potentially lower lability of peatland permafrost DOM[22]. This is in agreement with a recent study in central Siberia showing that DOM from previously frozen peat was highly refractory[65]. This highlights the unique nature of permafrost peatlands (19% of permafrost area, 70% in Eurasia, and more than one third of the organic carbon stocks[12]) with regards to post thaw organic carbon dynamics, in comparison to

370 mineral soils in the Arctic. This study indicates that a runaway feedback of old labile carbon
371 released as a result of permafrost thaw should not be expected in all cases. In peatland
372 permafrost, our results suggest that thawing carbon is highly aromatic, and might have
373 undergone previous microbial processing prior to permafrost aggradation. Permafrost peatlands
374 are therefore relatively unlikely to release labile DOM as a result of permafrost thaw.

375

376 ## ACKNOWLEDGMENT

377 This study was funded by CNRS - INEE through the PEPS program 'Blanc' 2015.
378 Travels to Igarka were supported by the SMI program of INPT. Additional support was
379 provided by the ERANet-LAC joint program (METHANOBASE ELAC2014_DCC-0092). A.
380 Hoyt was funded by the European Research Council (ERC) EU Horizon 2020 Programme
381 (grant No. 695101) and by the MIT-Russia Program of the MIT International Science and
382 Technology Initiative (MISTI). The DOC analysis were performed at the PAPC (Plateforme
383 d'Analyse Physico-Chimique) at the EcoLab Laboratory. The authors thank Franck Gilbert for
384 access to the spectofluorometer, Arnaud Mansat for the permafrost map, and Anatoly Pimov
385 for valuable logistical assistance in the field. The authors thank tree anonymous reviewers for
386 their constructive comments which improved the manuscript.

387 SUPPORTING INFORMATION.

388 Figure SI.1. Age of bulk OC in palsa mounts. Figure SI.2. Relationships between phenol ratios.
389 Figure SI.3 Plot of ^{14}C content versus DOC concentrations. Table SI.1. List of analyzed
390 compounds and m/z ratios used for their integration. This information is available free of charge
391 via the Internet at http://pubs.acs.org

392 ## REFERENCES

(1) Hugelius, G.; Strauss, J.; Zubrzycki, S.; Harden, J. W.; Schuur, E. a. G.; Ping, C.-L.; Schirrmeister, L.; Grosse, G.; Michaelson, G. J.; Koven, C. D.; et al. Estimated Stocks of Circumpolar Permafrost Carbon with Quantified Uncertainty Ranges and Identified Data Gaps. *Biogeosciences* **2014**, *11* (23), 6573–6593. https://doi.org/10.5194/bg-11-6573-2014.

(2) Schuur, E. A. G.; Bockheim, J.; Canadell, J. G.; Euskirchen, E.; Field, C. B.; Goryachkin, S. V.; Hagemann, S.; Kuhry, P.; Lafleur, P. M.; Lee, H.; et al. Vulnerability of Permafrost Carbon to Climate Change: Implications for the Global Carbon Cycle. *BioScience* **2008**, *58* (8), 701. https://doi.org/10.1641/B580807.

(3) Ciais, P.; Sabine, G.; Bala, G.; Bopp, L.; Brovkin, V.; Canadell, J. G.; Chhabra, A.; DeFries, R. S.; Galloway, J.; Heimann, M.; et al. Carbon and Other Biogeochemical Cycles. In: Climate Change 2013: The Physical Science Basis. In *Contribution of Working Group I to the Fifth Assessment Report of the Intergovernmental Panel on Climate Change*; Cambridge, United Kingdom and New York, NY, USA., 2013.

(4) Schuur, E. A. G.; McGuire, A. D.; Schädel, C.; Grosse, G.; Harden, J. W.; Hayes, D. J.; Hugelius, G.; Koven, C. D.; Kuhry, P.; Lawrence, D. M.; et al. Climate Change and the Permafrost Carbon Feedback. *Nature* **2015**, *520* (7546), 171–179. https://doi.org/10.1038/nature14338.

(5) Amon, R. M. W.; Rinehart, A. J.; Duan, S.; Louchouarn, P.; Prokushkin, A.; Guggenberger, G.; Bauch, D.; Stedmon, C.; Raymond, P. A.; Holmes, R. M.; et al. Dissolved Organic Matter Sources in Large Arctic Rivers. *Geochim. Cosmochim. Acta* **2012**, *94*, 217–237. https://doi.org/10.1016/j.gca.2012.07.015.

(6) Mann, P. J.; Eglinton, T. I.; McIntyre, C. P.; Zimov, N.; Davydova, A.; Vonk, J. E.; Holmes, R. M.; Spencer, R. G. M. Utilization of Ancient Permafrost Carbon in Headwaters of Arctic Fluvial Networks. *Nat. Commun.* **2015**, *6*, 7856. https://doi.org/10.1038/ncomms8856.

(7) Abbott, B. W.; Larouche, J. R.; Jones, J. B.; Bowden, W. B.; Balser, A. W. Elevated Dissolved Organic Carbon Biodegradability from Thawing and Collapsing Permafrost. *J. Geophys. Res. Biogeosciences* **2014**, *119* (10), 2014JG002678. https://doi.org/10.1002/2014JG002678.

(8) Raymond, P. A.; McClelland, J. W.; Holmes, R. M.; Zhulidov, A. V.; Mull, K.; Peterson, B. J.; Striegl, R. G.; Aiken, G. R.; Gurtovaya, T. Y. Flux and Age of Dissolved Organic Carbon Exported to the Arctic Ocean: A Carbon Isotopic Study of the Five Largest Arctic Rivers. *Glob. Biogeochem. Cycles* **2007**, *21* (4), GB4011. https://doi.org/10.1029/2007GB002934.

(9) O'Donnell, J. A.; Aiken, G. R.; Walvoord, M. A.; Raymond, P. A.; Butler, K. D.; Dornblaser, M. M.; Heckman, K. Using Dissolved Organic Matter Age and Composition to Detect Permafrost Thaw in Boreal Watersheds of Interior Alaska. *J. Geophys. Res. Biogeosciences* **2014**, *119* (11), 2155–2170. https://doi.org/10.1002/2014JG002695.

(10) Barnes, R. T.; Butman, D. E.; Wilson, H. F.; Raymond, P. A. Riverine Export of Aged Carbon Driven by Flow Path Depth and Residence Time. *Environ. Sci. Technol.* **2018**, *52* (3), 1028–1035. https://doi.org/10.1021/acs.est.7b04717.

(11) Drake, T. W.; Wickland, K. P.; Spencer, R. G. M.; McKnight, D. M.; Striegl, R. G. Ancient Low–Molecular-Weight Organic Acids in Permafrost Fuel Rapid Carbon Dioxide Production upon Thaw. *Proc. Natl. Acad. Sci.* **2015**, *112* (45), 13946–13951. https://doi.org/10.1073/pnas.1511705112.

(12) Tarnocai, C.; Canadell, J. G.; Schuur, E. a. G.; Kuhry, P.; Mazhitova, G.; Zimov, S. Soil Organic Carbon Pools in the Northern Circumpolar Permafrost Region. *Glob. Biogeochem. Cycles* **2009**, *23* (2). https://doi.org/10.1029/2008GB003327.

(13) Vallée, S.; Payette, S. Collapse of Permafrost Mounds along a Subarctic River over the Last 100 Years (Northern Québec). *Geomorphology* **2007**, *90* (1), 162–170. https://doi.org/10.1016/j.geomorph.2007.01.019.
(14) Borge, A. F.; Westermann, S.; Solheim, I.; Etzelmüller, B. Strong Degradation of Palsas and Peat Plateaus in Northern Norway during the Last 60 Years. *The Cryosphere* **2017**, *11* (1), 1–16. https://doi.org/10.5194/tc-11-1-2017.
(15) Swindles, G. T.; Morris, P. J.; Mullan, D.; Watson, E. J.; Turner, T. E.; Roland, T. P.; Amesbury, M. J.; Kokfelt, U.; Schoning, K.; Pratte, S.; et al. The Long-Term Fate of Permafrost Peatlands under Rapid Climate Warming. *Sci. Rep.* **2015**, *5*, 17951. https://doi.org/10.1038/srep17951.
(16) Hodgkins, S. B.; Tfaily, M. M.; Podgorski, D. C.; McCalley, C. K.; Saleska, S. R.; Crill, P. M.; Rich, V. I.; Chanton, J. P.; Cooper, W. T. Elemental Composition and Optical Properties Reveal Changes in Dissolved Organic Matter along a Permafrost Thaw Chronosequence in a Subarctic Peatland. *Geochim. Cosmochim. Acta* **2016**, *187*, 123–140. https://doi.org/10.1016/j.gca.2016.05.015.
(17) Pokrovsky, O. S.; Shirokova, L. S.; Kirpotin, S. N.; Audry, S.; Viers, J.; Dupré, B. Effect of Permafrost Thawing on Organic Carbon and Trace Element Colloidal Speciation in the Thermokarst Lakes of Western Siberia. *Biogeosciences* **2011**, *8* (3), 565–583. https://doi.org/10.5194/bg-8-565-2011.
(18) Wang, J.-J.; Lafrenière, M. J.; Lamoureux, S. F.; Simpson, A. J.; Gélinas, Y.; Simpson, M. J. Differences in Riverine and Pond Water Dissolved Organic Matter Composition and Sources in Canadian High Arctic Watersheds Affected by Active Layer Detachments. *Environ. Sci. Technol.* **2018**, *52* (3), 1062–1071. https://doi.org/10.1021/acs.est.7b05506.
(19) Olefeldt, D.; Roulet, N. T. Effects of Permafrost and Hydrology on the Composition and Transport of Dissolved Organic Carbon in a Subarctic Peatland Complex. *J. Geophys. Res. Biogeosciences* **2012**, *117* (G1), G01005. https://doi.org/10.1029/2011JG001819.
(20) Panneer Selvam, B.; Lapierre, J.-F.; Guillemette, F.; Voigt, C.; Lamprecht, R. E.; Biasi, C.; Christensen, T. R.; Martikainen, P. J.; Berggren, M. Degradation Potentials of Dissolved Organic Carbon (DOC) from Thawed Permafrost Peat. *Sci. Rep.* **2017**, *7*, 45811. https://doi.org/10.1038/srep45811.
(21) Treat, C. C.; Jones, M. C. Near-Surface Permafrost Aggradation in Northern Hemisphere Peatlands Shows Regional and Global Trends during the Past 6000 Years. *The Holocene* **2018**, *28* (6), 998–1010. https://doi.org/10.1177/0959683617752858.
(22) Treat, C. C.; Jones, M. C.; Camill, P.; Gallego-Sala, A.; Garneau, M.; Harden, J. W.; Hugelius, G.; Klein, E. S.; Kokfelt, U.; Kuhry, P.; et al. Effects of Permafrost Aggradation on Peat Properties as Determined from a Pan-Arctic Synthesis of Plant Macrofossils. *J. Geophys. Res. Biogeosciences* **2016**, *121* (1), 78–94. https://doi.org/10.1002/2015JG003061.
(23) Vonk, J. E.; Mann, P. J.; Davydov, S.; Davydova, A.; Spencer, R. G. M.; Schade, J.; Sobczak, W. V.; Zimov, N.; Zimov, S.; Bulygina, E.; et al. High Biolability of Ancient Permafrost Carbon upon Thaw: BIOLABILITY OF ANCIENT PERMAFROST CARBON. *Geophys. Res. Lett.* **2013**, *40* (11), 2689–2693. https://doi.org/10.1002/grl.50348.
(24) Streletskiy, D. A.; Tananaev, N. I.; Opel, T.; Shiklomanov, N. I.; Nyland, K. E.; Streletskaya, I. D.; Tokarev, I.; Shiklomanov, A. I. Permafrost Hydrology in Changing Climatic Conditions: Seasonal Variability of Stable Isotope Composition in Rivers in Discontinuous Permafrost. *Environ. Res. Lett.* **2015**, *10* (9), 095003. https://doi.org/10.1088/1748-9326/10/9/095003.

(25) Rodionov, A.; Flessa, H.; Grabe, M.; Kazansky, O. A.; Shibistova, O.; Guggenberger, G. Organic Carbon and Total Nitrogen Variability in Permafrost-affected Soils in a Forest Tundra Ecotone. *Eur. J. Soil Sci.* **2007**, *58* (6), 1260–1272. https://doi.org/10.1111/j.1365-2389.2007.00919.x.

(26) Kostyukevich, V. V. A Regional Geochronological Study of Late Pleistocene Permafrost. *Radiocarbon*. 1988, pp 477–486.

(27) Vasil'chuk, Y.; Vasil'chuk, A.; Jungner, H.; Budantseva, N.; Chizhova, J. Radiocarbon chronology of Holocene palsa of Bol'shezemel'skaya tundra in Russian North. https://ges.rgo.ru/jour/article/view/139 (accessed Jun 13, 2019).

(28) Liebner, S.; Ganzert, L.; Kiss, A.; Yang, S.; Wagner, D.; Svenning, M. M. Shifts in Methanogenic Community Composition and Methane Fluxes along the Degradation of Discontinuous Permafrost. *Front. Microbiol.* **2015**, *6*. https://doi.org/10.3389/fmicb.2015.00356.

(29) Johansson, T.; Malmer, N.; Crill, P. M.; Friborg, T.; åKerman, J. H.; Mastepanov, M.; Christensen, T. R. Decadal Vegetation Changes in a Northern Peatland, Greenhouse Gas Fluxes and Net Radiative Forcing. *Glob. Change Biol.* **2006**, *12* (12), 2352–2369. https://doi.org/10.1111/j.1365-2486.2006.01267.x.

(30) Weishaar, J. L.; Aiken, G. R.; Bergamaschi, B. A.; Fram, M. S.; Fujii, R.; Mopper, K. Evaluation of Specific Ultraviolet Absorbance as an Indicator of the Chemical Composition and Reactivity of Dissolved Organic Carbon. *Environ. Sci. Technol.* **2003**, *37* (20), 4702–4708. https://doi.org/10.1021/es030360x.

(31) McKnight, D. M.; Boyer, E. W.; Westerhoff, P. K.; Doran, P. T.; Kulbe, T.; Andersen, D. T. Spectrofluorometric Characterization of Dissolved Organic Matter for Indication of Precursor Organic Material and Aromaticity. *Limnol. Oceanogr.* **2001**, *46* (1), 38–48. https://doi.org/10.4319/lo.2001.46.1.0038.

(32) Jaffé R.; McKnight D.; Maie N.; Cory R.; McDowell W. H.; Campbell J. L. Spatial and Temporal Variations in DOM Composition in Ecosystems: The Importance of Long-term Monitoring of Optical Properties. *J. Geophys. Res. Biogeosciences* **2008**, *113* (G4). https://doi.org/10.1029/2008JG000683.

(33) Poulin, B. A.; Ryan, J. N.; Aiken, G. R. Effects of Iron on Optical Properties of Dissolved Organic Matter. *Environ. Sci. Technol.* **2014**, *48* (17), 10098–10106. https://doi.org/10.1021/es502670r.

(34) Synal, H.-A.; Stocker, M.; Suter, M. MICADAS: A New Compact Radiocarbon AMS System. *Nucl. Instrum. Methods Phys. Res. Sect. B Beam Interact. Mater. At.* **2007**, *259* (1), 7–13. https://doi.org/10.1016/j.nimb.2007.01.138.

(35) Ruff, M.; Fahrni, S.; Gäggeler, H. W.; Hajdas, I.; Suter, M.; Synal, H.-A.; Szidat, S.; Wacker, L. On-Line Radiocarbon Measurements of Small Samples Using Elemental Analyzer and MICADAS Gas Ion Source. *Radiocarbon* **2010**, *52* (4), 1645–1656. https://doi.org/10.1017/S003382220005637X.

(36) Stuiver, M.; Polach, H. A. Discussion Reporting of 14C Data. *Radiocarbon* **1977**, *19* (3), 355–363. https://doi.org/10.1017/S0033822200003672.

(37) Reimer, P. J.; Baillie, M. G. L.; Bard, E.; Bayliss, A.; Beck, W.; Bertrand, C.; Blackwell, P. G.; Buck, C. E.; Burr, G. S.; Cutler, K. B.; et al. Intcal04 Terrestrial Radiocarbon Age Calibration, 0–26 Cal Kyr BP. *Radiocarbon* **2004**, *46* (3), 1029–1058. https://doi.org/10.1017/S0033822200032999.

(38) Graven, H.; Allison, C.; Etheridge, D.; Hammer, S.; Keeling, R.; Levin, I.; Meijer, H.; Rubino, M.; Tans, P.; Trudinger, C.; et al. Compiled Records of Carbon Isotopes in Atmospheric CO2 for Historical Simulations in CMIP6. *Geosci. Model Dev.* **2017**. http://dx.doi.org/10.5194/gmd-10-4405-2017.

(39) Jeanneau, L.; Denis, M.; Pierson-Wickmann, A.-C.; Gruau, G.; Lambert, T.; Petitjean, P. Sources of Dissolved Organic Matter during Storm and Inter-Storm Conditions in a Lowland Headwater Catchment: Constraints from High-Frequency Molecular Data. *Biogeosciences* **2014**, *12* (14), 4333–4343. https://doi.org/10.5194/bg-12-4333-2015.

(40) Nierop, K. G. J.; Preston, C. M.; Kaal, J. Thermally Assisted Hydrolysis and Methylation of Purified Tannins from Plants. *Anal. Chem.* **2005**, *77* (17), 5604–5614. https://doi.org/10.1021/ac050564r.

(41) Grasset, L.; Rovira, P.; Amblès, A. TMAH-Preparative Thermochemolysis for the Characterization of Organic Matter in Densimetric Fractions of a Mediterranean Forest Soil. *J. Anal. Appl. Pyrolysis* **2009**, *85* (1), 435–441. https://doi.org/10.1016/j.jaap.2008.09.004.

(42) Frostegård, Å.; Tunlid, A.; Bååth, E. Phospholipid Fatty Acid Composition, Biomass, and Activity of Microbial Communities from Two Soil Types Experimentally Exposed to Different Heavy Metals. *Appl Env. Microbiol* **1993**, *59* (11), 3605–3617.

(43) Rumpel, C.; Dignac, M.-F. Gas Chromatographic Analysis of Monosaccharides in a Forest Soil Profile: Analysis by Gas Chromatography after Trifluoroacetic Acid Hydrolysis and Reduction–Acetylation. *Soil Biol. Biochem.* **2006**, *38* (6), 1478–1481. https://doi.org/10.1016/j.soilbio.2005.09.017.

(44) Goñi, M. A.; Hedges, J. I. Lignin Dimers: Structures, Distribution, and Potential Geochemical Applications. *Geochim. Cosmochim. Acta* **1992**, *56* (11), 4025–4043. https://doi.org/10.1016/0016-7037(92)90014-A.

(45) Kögel, I. Estimation and Decomposition Pattern of the Lignin Component in Forest Humus Layers. *Soil Biol. Biochem.* **1986**, *18* (6), 589–594. https://doi.org/10.1016/0038-0717(86)90080-5.

(46) R Core Team. A Language and Environment for Statistical Computing, R Foundation for Statistical Computing, Vienna, Austria (Http://R-Project.Org/). (http://R-project.org/) 2019.

(47) Wickham, H. Ggplot2: Elegant Graphics for Data Analysis. Springer-Verlag New York 2016.

(48) Wickham, H.; François, R.; Henry, L.; Müller, K. Dplyr: A Grammar of Data Manipulation. R Package Version 0.8.0.1. Https://CRAN.R-Project.Org/Package=dplyr. 2019.

(49) Dinno, A. Dunn.Test: Dunn's Test of Multiple Comparisons Using Rank Sums. R Package Version 1.3.5. Https://CRAN.R-Project.Org/Package=dunn.Test. 2017.

(50) McKnight, D. M.; Boyer, E. W.; Westerhoff, P. K.; Doran, P. T.; Kulbe, T.; Andersen, D. T. Spectrofluorometric Characterization of Dissolved Organic Matter for Indication of Precursor Organic Material and Aromaticity. *Limnol. Oceanogr.* **2001**, *46* (1), 38–48. https://doi.org/10.4319/lo.2001.46.1.0038.

(51) Hernes, P. J.; Benner, R. Photochemical and Microbial Degradation of Dissolved Lignin Phenols: Implications for the Fate of Terrigenous Dissolved Organic Matter in Marine Environments. *J. Geophys. Res. Oceans* **2003**, *108* (C9). https://doi.org/10.1029/2002JC001421.

(52) Spencer, R. G. M.; Stubbins, A.; Hernes, P. J.; Baker, A.; Mopper, K.; Aufdenkampe, A. K.; Dyda, R. Y.; Mwamba, V. L.; Mangangu, A. M.; Wabakanghanzi, J. N.; et al. Photochemical Degradation of Dissolved Organic Matter and Dissolved Lignin Phenols from the Congo River. *J. Geophys. Res. Biogeosciences* **2009**, *114* (G3). https://doi.org/10.1029/2009JG000968.

(53) Laurion, I.; Mladenov, N. Dissolved Organic Matter Photolysis in Canadian Arctic Thaw Ponds. *Environ. Res. Lett.* **2013**, *8* (3), 035026. https://doi.org/10.1088/1748-9326/8/3/035026.

(54) Ward, C. P.; Cory, R. M. Complete and Partial Photo-Oxidation of Dissolved Organic Matter Draining Permafrost Soils. *Environ. Sci. Technol.* **2016**, *50* (7), 3545–3553. https://doi.org/10.1021/acs.est.5b05354.

(55) Marschner, B.; Kalbitz, K. Controls of Bioavailability and Biodegradability of Dissolved Organic Matter in Soils. *Geoderma* **2003**, *113* (3–4), 211–235. https://doi.org/10.1016/S0016-7061(02)00362-2.

(56) Lee, M.-H.; Osburn, C. L.; Shin, K.-H.; Hur, J. New Insight into the Applicability of Spectroscopic Indices for Dissolved Organic Matter (DOM) Source Discrimination in Aquatic Systems Affected by Biogeochemical Processes. *Water Res.* **2018**, *147*, 164–176. https://doi.org/10.1016/j.watres.2018.09.048.

(57) Abbott, B. W.; Larouche, J. R.; Jones, J. B.; Bowden, W. B.; Balser, A. W. Elevated Dissolved Organic Carbon Biodegradability from Thawing and Collapsing Permafrost: Permafrost Carbon Biodegradability. *J. Geophys. Res. Biogeosciences* **2014**, *119* (10), 2049–2063. https://doi.org/10.1002/2014JG002678.

(58) Estop-Aragonés, C.; Czimczik, C. I.; Heffernan, L.; Gibson, C.; Walker, J. C.; Xu, X.; Olefeldt, D. Respiration of Aged Soil Carbon during Fall in Permafrost Peatlands Enhanced by Active Layer Deepening Following Wildfire but Limited Following Thermokarst. *Environ. Res. Lett.* **2018**, *13* (8), 085002. https://doi.org/10.1088/1748-9326/aad5f0.

(59) Vonk, J.; Tank, S.; Mann, P.; Spencer, R.; Treat, C.; Striegl, R.; Abbott, B.; Wickland, K. Biodegradability of Dissolved Organic Carbon in Permafrost Soils and Aquatic Systems: A Meta-Analysis. *Biogeosciences BG* **2015**, *12*, 6915–6930.

(60) Estop-Aragonés, C.; Cooper, M. D. A.; Fisher, J. P.; Thierry, A.; Garnett, M. H.; Charman, D. J.; Murton, J. B.; Phoenix, G. K.; Treharne, R.; Sanderson, N. K.; et al. Limited Release of Previously-Frozen C and Increased New Peat Formation after Thaw in Permafrost Peatlands. *Soil Biol. Biochem.* **2018**, *118*, 115–129. https://doi.org/10.1016/j.soilbio.2017.12.010.

(61) Spencer, R. G. M.; Mann, P. J.; Dittmar, T.; Eglinton, T. I.; McIntyre, C.; Holmes, R. M.; Zimov, N.; Stubbins, A. Detecting the Signature of Permafrost Thaw in Arctic Rivers. *J. Geophys. Res. Oceans* **2016**, 2830–2835. https://doi.org/10.1002/2015GL063498@10.1002/(ISSN)2169-9291.ARCTICJOINT.

(62) Mann, P. J.; Eglinton, T. I.; McIntyre, C. P.; Zimov, N.; Davydova, A.; Vonk, J. E.; Holmes, R. M.; Spencer, R. G. M. Utilization of Ancient Permafrost Carbon in Headwaters of Arctic Fluvial Networks. *Nat. Commun.* **2015**, *6*, 7856. https://doi.org/10.1038/ncomms8856.

(63) Ewing, S. A.; O'Donnell, J. A.; Aiken, G. R.; Butler, K.; Butman, D.; Windham-Myers, L.; Kanevskiy, M. Z. Long-Term Anoxia and Release of Ancient, Labile Carbon upon Thaw of Pleistocene Permafrost. *Geophys. Res. Lett.* **2015**, *42* (24), 10,730-10,738. https://doi.org/10.1002/2015GL066296.

(64) Hansen, A. M.; Kraus, T. E. C.; Pellerin, B. A.; Fleck, J. A.; Downing, B. D.; Bergamaschi, B. A. Optical Properties of Dissolved Organic Matter (DOM): Effects of Biological and Photolytic Degradation. *Limnol. Oceanogr.* **2016**, *61* (3), 1015–1032. https://doi.org/10.1002/lno.10270.

(65) Shirokova, L. S.; Chupakov, A. V.; Zabelina, S. A.; Neverova, N. V.; Payandi-Rolland, D.; Causserand, C.; Karlsson, J.; Pokrovsky, O. S. Humic Surface Waters of Frozen Peat Bogs (Permafrost Zone) Are Highly Resistant to Bio- and Photodegradation. *Biogeosciences* **2019**, *16* (12), 2511–2526. https://doi.org/10.5194/bg-16-2511-2019.

639

640 **Table 1.** General water quality (pH, conductivity), DOC concentrations, optical properties (FI and SUVA); and $\delta^{13}C$- signature of DOM in

641 porewater of thermokarst bogs and surface water of thermokarst lakes. sd: Standard deviation.

	n	pH	Cond. (µS cm^{-1})	DOC (mg L^{-1})	FI	SUVA (L mgC^{-1} m^{-1})	$\delta^{13}C$-DOC (‰)
Small bogs	10	4.5±0.2	69±40	44.1±10.1	1.35±0.06	5.36±0.60	-27.7±0.3
Large bogs	12	5.0±1.0	82±38	16.7±1.2	1.51±0.06	4.81±0.34	-29.0±0.8
Fens	8	5.7±1.2	47±48	11.0±2.4	1.55±0.06	4.83±0.63	-28.5±1.1
Therm. Lakes	12	4.6±0.9	40±36	14.0±4.2	1.5±0.05	4.88±0.48	-28.8±1.0
Mineral Bog	9	5.4±0.6	44 ±24	12.9±2.3	1.64±0.05	4.28±0.80	-29.4±0.3

642

643

644

645 **Table 2.** DOM molecular analysis in porewater of thermokarst bogs and lakes (mean±sd). SA: small acids, CAR: carbohydrates, FA: fatty acids,
646 PHE: phenolic compounds, LMWFA: low molecular weight fatty acids, pcVEG: percentage of vegetation, C/V: ratio of cinnamyl to vanillyl acids,
647 S/V: ratio of syringyl to vanillyl acids, $(Al/Ac)_V$: ratio of aldehyde to acid moieties for vanillyl, $(Al/Ac)_S$: aldehyde to acid moieties for syringyl.

	CAR	FA	LMWFA	pcVEG	C/V	S/V	(Al/Ac)v	(Al/Ac)s
SB	31.2±0.4	3.9±0.8	47.6±5.5	86.3±8.2	78.0±5.0	0.10±0.0	0.38±0.1	0.10±0.0
LB	20.0±4.9	6.1±3.0	39.5±6.0	65.8±21.3	70.6±6.7	0.50±0.2	0.43±0.1	0.21±0.1
MB	23.6±4.6	3.3±0.4	45.1±3.2	83.5±11.0	69.5±6.6	0.32±0.1	0.45±0.0	0.13±0.0
Lake	23.7±5.7	8.0±0.4	56.0±4.2	96.5±0.1	81.5±0.7	0.13±0.0	0.29±0.1	0.08±0.0

648

649

650

651 **Table 3.** Relationships between radiocarbon content of DOM and SUVA index for this study
652 and reported results from the literature.

Study	Scale	Geological Context	SUVA = $aF^{14}C+b$
This study	Thermokarst bogs pore water profile	Holocene peatlands	y = -4.78 x + 9.53 r^2 = 0.55, n=21 , p<0.001
Mann et al., 2015	Thaw water, streams	Yedoma	y = 2.23 x + 1.29 r^2 = 0.78, n= 23, p<0.0001
Barnes et al., 2018	Yeniseï River	Yenissei watershed	y = 5.90 x - 3.14 r^2 = 0.25, n=45, p<0.001
Wang et al., 2018	Pond waters	High Canadian Arctic	y = 8.17 x - 3.36 r^2 = 0.38, n=15, p<0.05

653

654

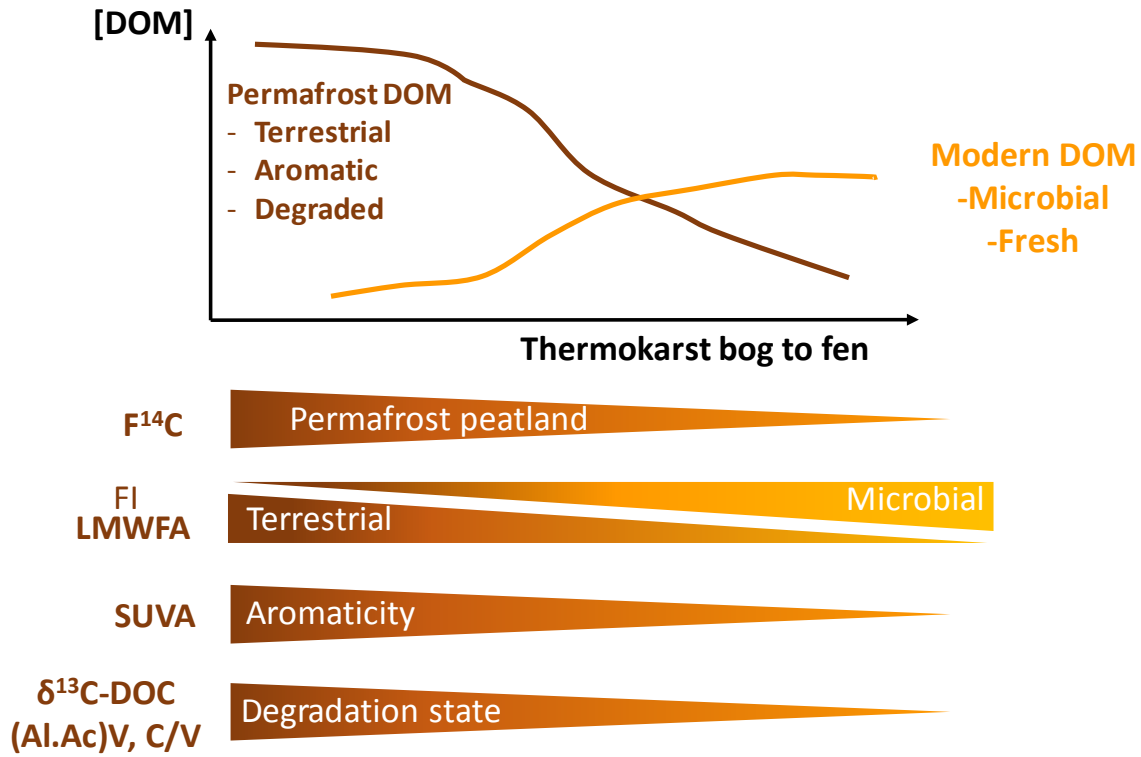

Graphical abstract.

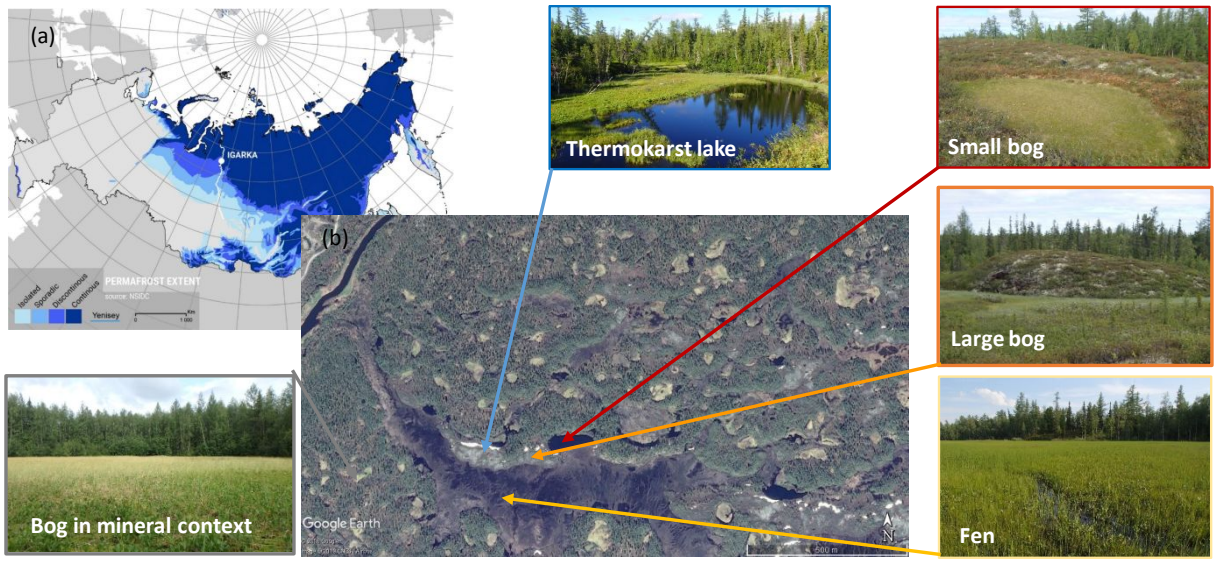

Figure 1. (a) Location of Igarka and permafrost status in the Republic of Russia. (b) Sampling area, with location of sampling points. Pictures are representative of sampling locations. Data from IPA (International Permafrost Association) and Google Earth.

686

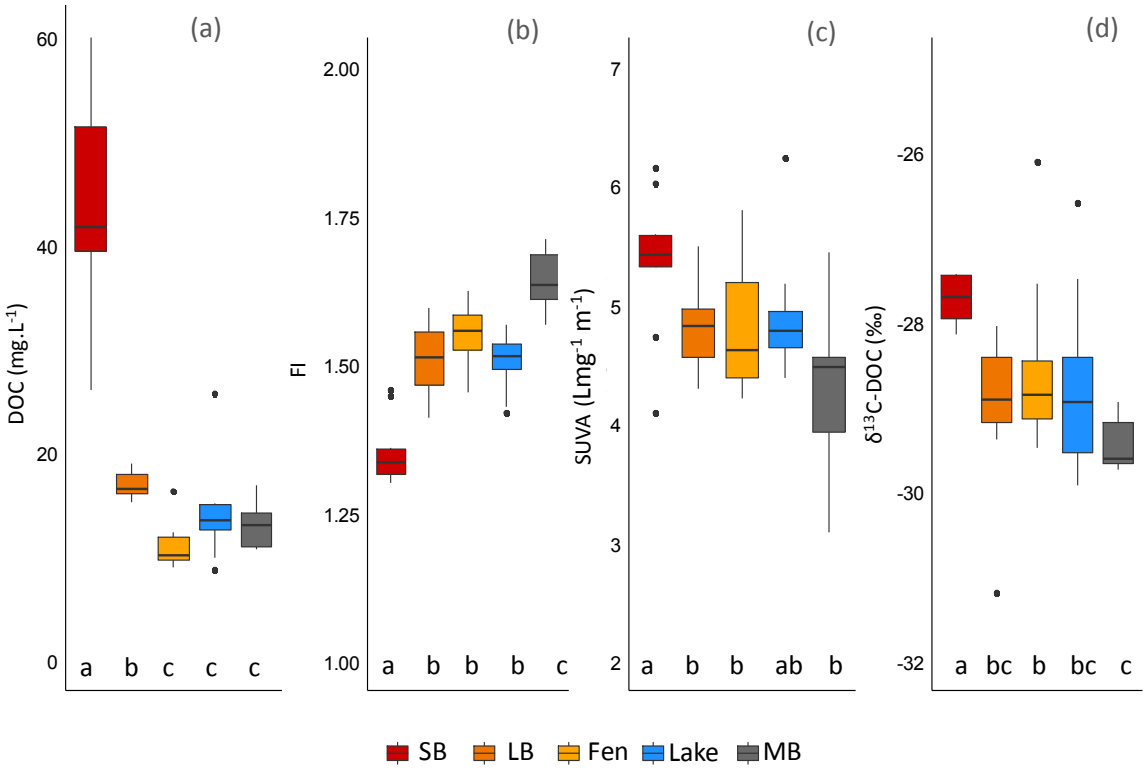

687

688 **Figure 2**. (a) DOC concentration, (b) Fluorescence Index (FI), (c) Specific UV Absorbance

689 (SUVA) and (d) $\delta^{13}C$ of DOM of the different sample types. The black line is the

690 median. The lower and upper levels of the box represent the 25 and 75 % quartile,

691 respectively. The lower whisker is smallest observation greater than or equal to lower

692 hinge - 1.5 * IQR (inter-quartile range), the upper whisker, the upper whisker is the

693 largest observation less than or equal to upper hinge + 1.5 * IQR. SB= small bogs, LB

694 = large bogs, lake = thermokarst lake, MB = thermokarst bog developed in mineral

695 context. Letters represent significantly different groups (Kruskall Wallis and Dunn's

696 post hoc multiple test ($p>0.05$)).

697

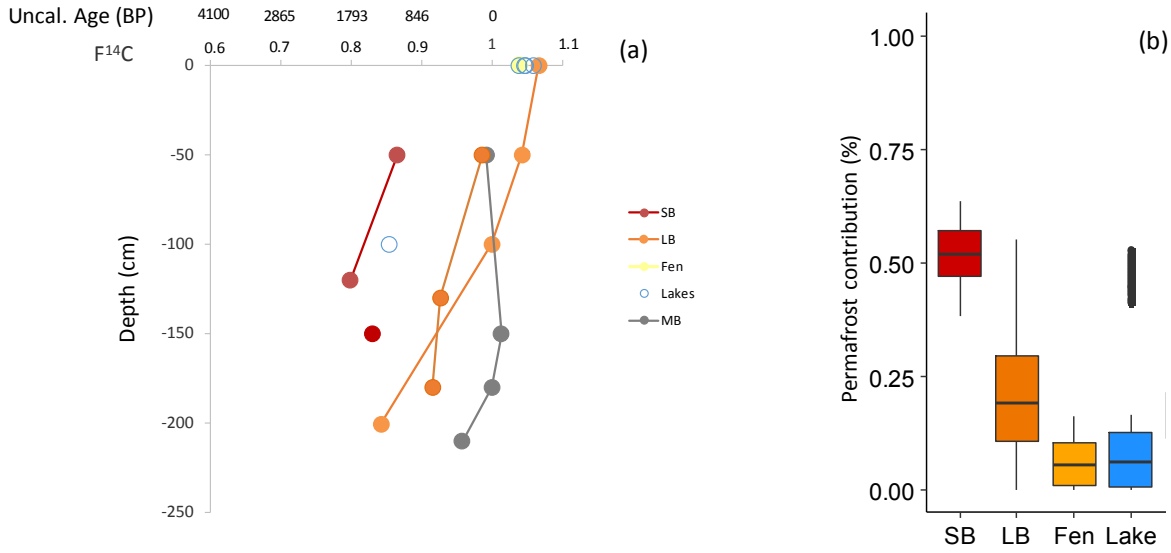

Figure 3. (a) Profiles of radiocarbon content of selected samples of DOM in thermokarst bogs profiles, porewater surface, sediment porewater of lake and surface water of lakes. (b) Proportion of permafrost to DOM. The distribution corresponds to calculation with atmospheric signature ranging from 1980 to 2015 (sampling date). SB= small bogs, LB = large bogs, Lake = thermokarst lake, MB = thermokarst bog developed in mineral context.

715

716

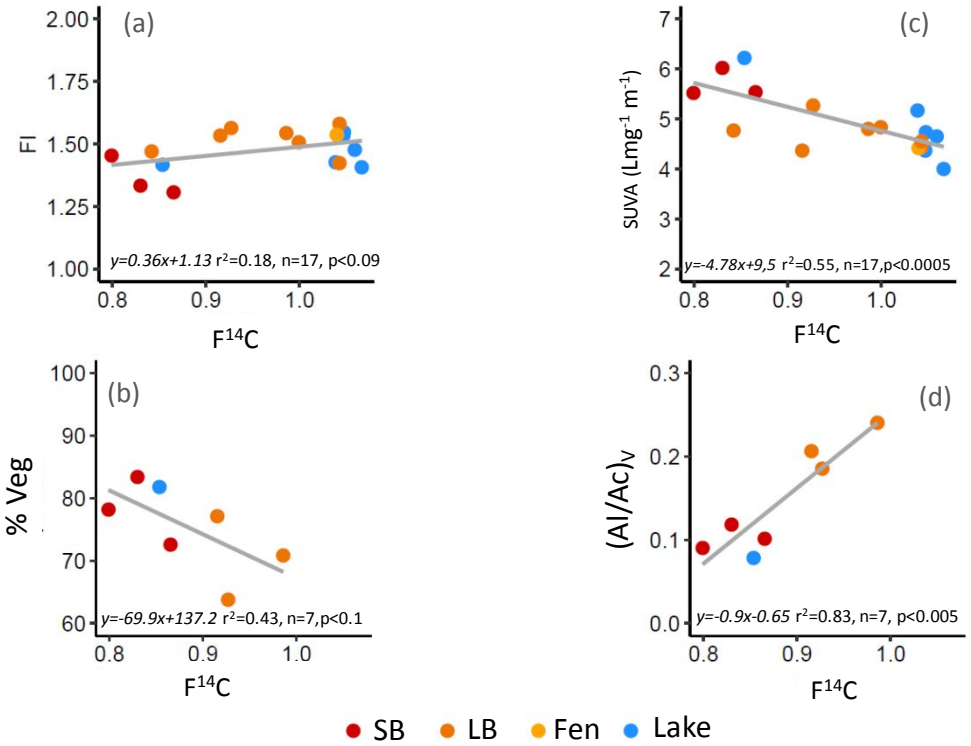

717

718

719 **Figure 4**. Relationship between radiocarbon content of DOM with (a) FI (Fluorescence Index), (b),
720 SUVA (Specific UV Absorbance), (c) percentage of vegetation origin of DOM, (d)
721 $(Al/Ac)_V$: ratio of aldehyde to acid moieties for vanillyl. SB= small bogs, LB = large bogs, Lake
722 = thermokarst lake.

723

724

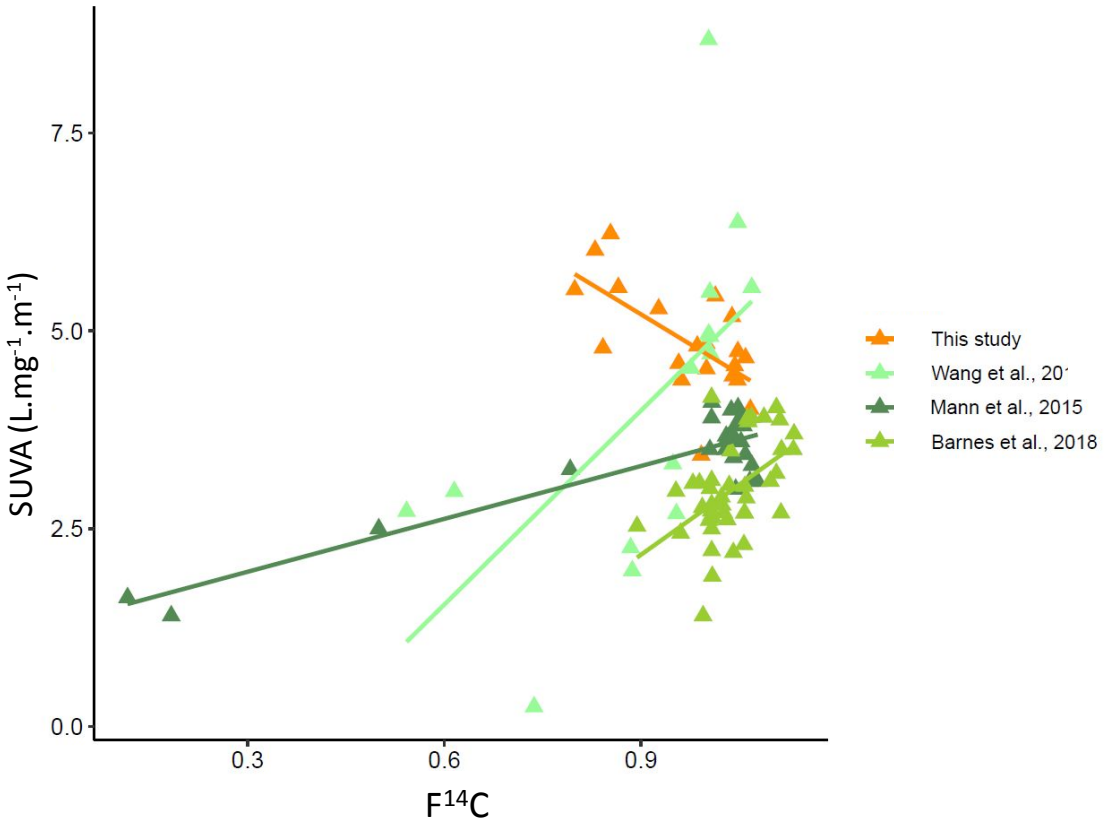

Figure 5: Relationship radiocarbon content of DOM and SUVA in different geological contexts and at different scales. (Wang et al., 2018 : High Arctic ponds, Mann et al., 2015 : Streams and thaw water in Yedoma Context, Barnes et al., 2018 : Yenisei watershed).